processes

MDPI

Article

Hydrodynamic Study of AR Coupling Effects on Solid Circulation and Gas Leakages in a High-Flux In Situ Gasification Chemical Looping Combustion System

Xiaojia Wang *, Xianli Liu, Baosheng Jin and Decheng Wang

Key Laboratory of Energy Thermal Conversion and Control of Ministry of Education, School of Energy and Environment, Southeast University, Nanjing 210096, China; liuxl_seu@163.com (X.L.); bsjin@seu.edu.cn (B.J.); dechengw76@126.com (D.W.)

* Correspondence: xiaojiawang@seu.edu.cn

Received: 27 September 2018; Accepted: 16 October 2018; Published: 18 October 2018

Abstract: In situ gasification chemical looping combustion (iG-CLC) is a novel and promising coal combustion technology with inherent separation of CO_2. Our previous studies demonstrated the feasibility of performing iG-CLC with a high-flux circulating fluidized bed (HFCFB) riser as the fuel reactor (FR) and a counter-flow moving bed (CFMB) as the air reactor (AR). As an extension of that work, this study aims to further investigate the fundamental effects of the AR coupling on the oxygen carrier (OC) circulation and gas leakages with a cold-state experimental device of the proposed iG-CLC system. The system exhibited favorable pressure distribution characteristics and good adaptability of solid circulation flux, demonstrating the positive role of the direct coupling method of the AR in the stabilization and controllability of the whole system. The OC circulation and the gas leakages were mainly determined by the upper and lower pressure gradients of the AR. With the increase in the upper pressure gradient, the OC circulation flux increased initially and later decreased until the circulation collapsed. Besides, the upper pressure gradient exhibited a positive effect on the restraint of gas leakage from the FR to the AR, but a negative effect on the suppression of gas leakage from the AR to the FR. Moreover, the gas leakage of the J-valve to the AR, which is directly related to the solid circulation stability, was exacerbated with the increase of the lower pressure gradient of the AR. In real iG-CLC applications, the pressure gradients should be adjusted flexibly and optimally to guarantee a balanced OC circulation together with an ideal balance of all the gas leakages.

Keywords: in situ gasification chemical looping combustion; high-flux circulating fluidized bed; counter-flow moving bed; gas leakage; coupling mechanism

1. Introduction

Chemical looping combustion (CLC), which possesses an inherent feature of isolating CO_2 during the combustion process, has been regarded as a promising novel combustion technology with a low energy penalty for carbon capture [1,2]. A conventional CLC system is mainly comprised of a fuel reactor (FR) and an air reactor (AR). The fuel introduced into the FR is oxidized to CO_2 and H_2O by a solid oxygen carrier (OC). The reduced OC particles are then transferred to the AR where they are re-oxidized upon contact with air. Compared to conventional combustion methods, the fuel will no longer mix with N_2 in a CLC process, by means of the circulation of OC between the two reactors. Therefore, the flue gas leaving the FR will only contain CO_2 and H_2O with a complete conversion of the fuel, which enables efficient and energy-saving CO_2 capture via the condensation of H_2O [3,4].

On the basis of fuel types, CLC technology can be broadly categorized into gas-fueled CLC and solid-fueled CLC. So far, studies on gas-fueled CLC have been extensively conducted in different prototype reactors [5–14]. In recent years, considering the price advantage of solid fuels (coal as the main representative) in comparison with those of gaseous fuels, solid-fueled CLC began to attract increasing attention [15–21]. One of the coal-fueled CLC approaches is the so-called in situ gasification chemical looping combustion (iG-CLC) which involves three reaction steps between two reactors [20,21]. As shown in Figure 1, two of the reaction steps occur in the FR, i.e., the coal gasification reaction (Step 1) and the subsequent oxidation reactions of the gasification gases by the OC (Step 2). The other reaction step proceeds in the AR, i.e., the reoxidation reaction of the OC by air (Step 3).

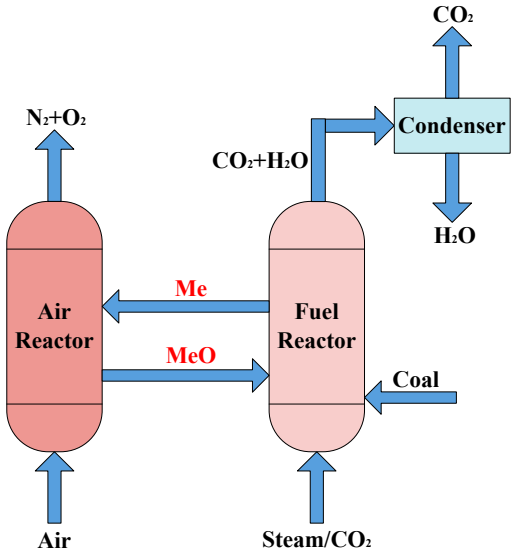

Figure 1. Schematic diagram of an in situ gasification chemical looping combustion (iG-CLC) system.

Up to now, some experimental studies on iG-CLC systems have been carried out with various reactor designs [16,18,22–28]. An iG-CLC configuration with a bubbling fluidized bed (BFB) as the FR and a circulating fluidized bed (CFB) as the AR was first proposed by Berguerand and Lyngfelt [16] from Chalmers University of Technology (10 kW_{th}), in view of the advantages of sufficient solid residence time in the BFB and favorable gas-solid contact in the CFB. Still, with CFBs as the ARs, some other FR designs have also been put forward. Shen et al. [18] from Southeast University adopted a spout-fluid bed (SFB) instead of the BFB as the FR (10 kW_{th}), in which the strong solid mixing enhanced the gas-solid contact and reaction efficiencies. Thon et al. [22] from Hamburg University of Technology designed a two-stage BFB as the FR (25 kW_{th}) for the purpose of enhancing the conversion of combustible gases. Bayham et al. [23] from Ohio State University utilized a counter-current moving bed as the FR (25 kW_{th}) with OC particles flowing downwards and gases flowing upwards, showing high competitiveness in the combustion performance and CO_2 purity. Adánez et al. [24] from CSIC proposed a CFB as the FR (20 kW_{th}) in order to achieve intense gas-solid contact and reaction. This kind of dual circulating fluidized bed (DCFB) design (i.e., both the FR and AR are CFBs) can also be found in the units by Markström et al. [25] from Chalmers University of Technology (100 kW_{th}), Ma et al. [26] from Huazhong University of Science and Technology (5 kW_{th}), and Ströhle et al. [27] from Technische Universität Darmstadt (1 MW_{th}). In addition, some other units with different design concepts have also been constructed and operated. Xiao et al. [28] from Southeast University developed a 50 kW_{th} iG-CLC unit where the AR and FR were designed as a BFB and a CFB, respectively. Pressurized conditions were achieved in their work, demonstrating the positive role of high-pressure operation in carbon conversion, CO_2 capture concentration, and combustion efficiency.

In our previous studies, we also proposed an iG-CLC system based on the high-flux circulating fluidized bed (HFCFB) technology [29–32]. Specifically, an HFCFB riser was designed as the FR

because it can provide not only a favorable gas-solid contact but also sufficient solid holdups over the whole reactor height, which should be very beneficial to the interphase reaction efficiency. Specifically, compared to the common CFB FRs [24–27], the higher OC inventory in this HFCFB FR can potentially compensate for the low reactivity of OC to a certain degree, and hence this high-flux iG-CLC system will have a large advantage on the operation cost by virtue of the use of low-grade natural iron ores with a lower reactivity than the OCs. Certainly, the high-flux operation will inevitably lead to a higher pressure drop. Therefore, greater energy consumption is required to compensate for the pressure loss. However, compared to the cost reduction from the use of cheap OCs, the slight increase in energy consumption should be acceptable. A counter-flow moving bed (CFMB), in view of its advantages of steady solid flow, low pressure drop, and compact structure, was employed as the AR. Besides, it can be simply placed in the middle of the HFCFB downcomer to enhance the simplicity and stabilization of the whole system. Moreover, an inertial separator-based carbon stripper was specially designed to separate the reduced OC from the FR to the AR for reoxidation, and recirculate the unconverted char for further conversion.

Based on the design concept of this high-flux iG-CLC system, we successively built and tested a cold visualization experimental device operating at the ambient temperature [30,31] and a hot pilot-scale 20 kW_{th} unit operating at the high-temperature conditions between 800–1000 °C [32]. After a series of tests, the steady operation with favorable gas-solid flow and reaction performance of the whole system could be realized under certain conditions, preliminarily verifying the feasibility of this design. With the deepening of the research, we have found that, compared to most iG-CLC systems with indirect serial structures of the two reactors [16,24–28], the direct coupling of the CFMB AR into the downcomer of the HFCFB FR in our system indeed contributes to the stabilization and controllability of the whole system. However, this coupling method of the AR also inevitably brings about greater challenges on the control of gas leakages between the two reactors, which will, in turn, affect the matching principle of reactors, such as the OC circulation characteristics.

The aim of this study is to investigate the fundamental effects of the AR coupling on the system operation stability and gas leakages. The pressure distribution characteristics of the whole system and the adaptability of solid circulation flux were first investigated with the cold-state visualization device for the proposed iG-CLC system. The effects of the upper and lower pressure gradients of the AR on the OC circulation and the gas leakages were further established. Moreover, by giving consideration to the AR coupling effects under various operational conditions, one optimal operating condition was recommended to demonstrate the adjustment feasibility for balanced solids circulation with low gas leakages during the iG-CLC process.

2. Materials and Methods

2.1. Experimental Device

Figure 2 gives a schematic representation of the experimental device for the proposed iG-CLC system under cold conditions. Here, only a brief description of the experimental setup is provided. A more detailed description can be found in our initial studies of this system [31].

2.1.1. Main Assembly

The main assembly predominantly consists of a FR (5), a carbon stripper (6), a downcomer (7), an AR (8), a J-valve (11), and a bag filter (12).

The FR (5) is an HFCFB riser with a height of 5.8 m and an inner diameter of 60 mm. The AR (8) is a CFMB, mainly consisting of a gas inlet (10), a gas outlet (9), a cylindrical channel (0.418 m inner diameter × 0.5 m height), and a cone channel (0.2 m height). The carbon stripper (6) is an inertial separator. For the purpose of visualization, some sections of the FR, the AR, and the downcomer are made of plexiglas.

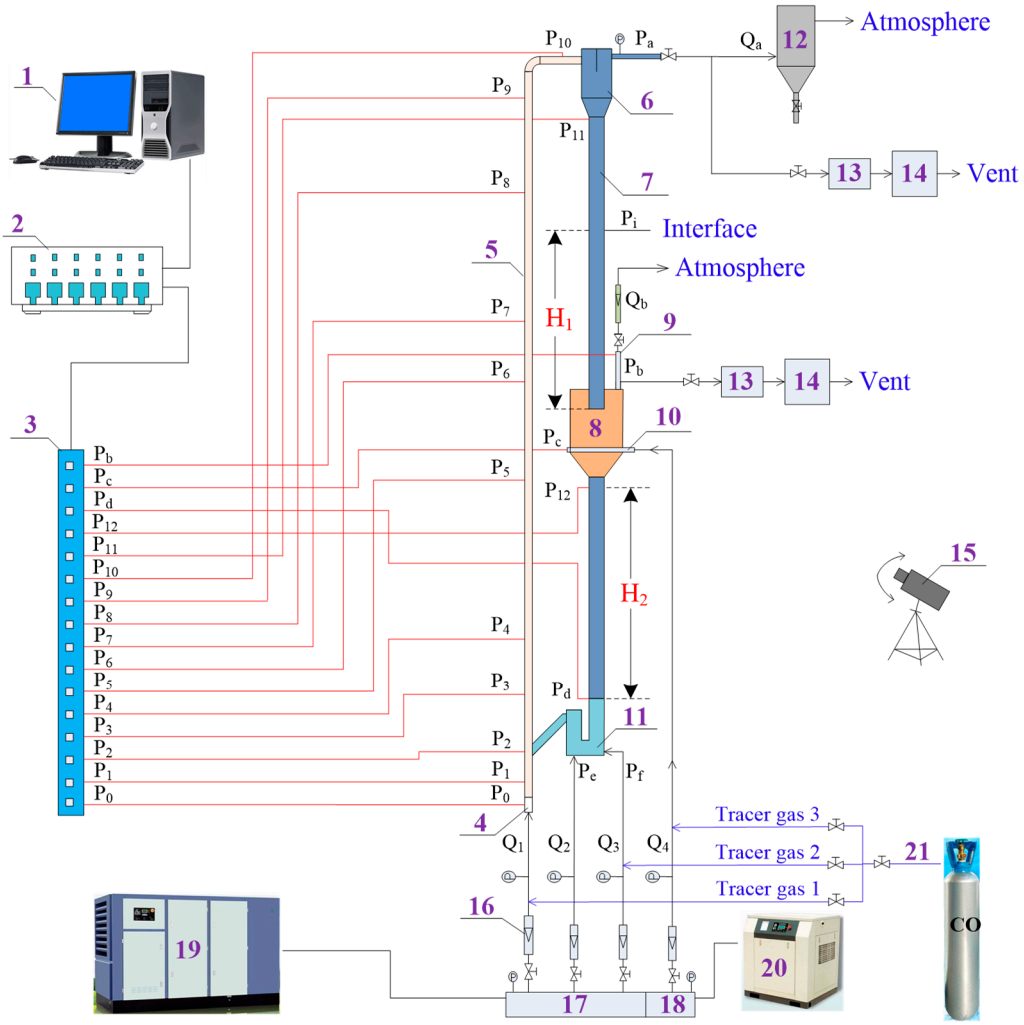

Figure 2. Schematic of the visualization experimental device of the iG-CLC system. 1—computer, 2—A/D converter, 3—differential pressure transducer, 4—riser gas chamber, 5—fuel reactor (FR), 6—carbon stripper, 7—downcomer, 8—air reactor (AR), 9—AR gas outlet, 10—AR gas inlet, 11—J-valve, 12—bag filter, 13—filter, 14—gas analyzer, 15—digital camera, 16—rotameter, 17—FR gas chamber, 18—AR gas chamber, 19—90 kW air compressor, 20—18 kW air compressor, 21—tracer gas. P—pressure gauge, Q—gas flow.

2.1.2. Gas Supply System

The air stream from a 90 kW air compressor (Nanjing Compressor Co. Ltd., Nanjing, China) (19) was introduced into the FR to circulate the OC particles. Another air stream from an 18 kW air compressor (Guangzhou Panyu JOYO Air Compressor Factory, Guangzhou, China) (20) was fed into the AR through a tube distributor.

A high-purity carbon monoxide (99.99%) stream was used as the tracer gas (21) which would be fed into the FR, the AR, and the J-valve in turn during the testing stages.

2.1.3. Data Acquisition System

Gas flow rates in the FR, AR, and J-valve were controlled and measured by calibrated rotameters (16).

The pressures of monitoring nodes were measured by pressure manometers and a multi-channel differential pressure transducer (3). During the experiments, the pressures of the two reactors could be adjusted by back-pressure regulators.

The tracer gas concentrations at the outlets of the two reactors were measured by a gas analyzer (MRU, Neckarsulm, Germany) (14).

A digital camera (15) was used to photograph the flow regimes and capture some special flow phenomena through the visualization sections during the experiments.

2.2. Material

The OC used in this study was a natural iron ore from Harbin, China. Prior to the experiments, the OC particles were crushed and sieved to a mean diameter of 0.43 mm. More details on this OC material can be found in Table 1.

Table 1. Main physical properties of the oxygen carrier.

Description	Value	
	Diameter (mm)	**Mass Fraction (%)**
Particle size distribution	>1.25	0.05
	1–1.25	0.71
	0.6–1	2.79
	0.45–0.6	22.94
	0.4–0.45	45.14
	0.3–0.4	22.94
	<0.3	5.43
Mean diameter d_p (mm)	0.43	-
Apparent density ρ_s (kg/m^3)	3015	-
Bulk density ρ_b (kg/m^3)	1577	-
Minimum fluidization gas velocity U_{mf} (m/s)	0.187	-

2.3. Experimental Procedures

The particles of the OC were first packed in the downcomer. Then, the gas stream from the 90 kW air compressor was introduced into the FR from the J-valve and FR distributor to drive the OC particles for circulation. After the particle circulation became balanced, another gas stream from the 18 kW air compressor was introduced into the AR and coupled into the original circulation system. As the system rebounded to a steady state, the effects of operating parameters began to be tested with the real-time monitoring of the system flow state, by means of pressure tracking, time sampling, gas tracer, and so on. A detailed explanation of the data processing can be found in Section 2.4.

2.4. Data Evaluation

2.4.1. Gas Flow Rates

The gas flow rates in this study were all normalized to the standard state with the subscript *sta*. According to the conservation of mass, the total gas flow rate of the system can be calculated as [31]

$$Q_{in,sta} = Q_{1,sta} + Q_{2,sta} + Q_{3,sta} + Q_{4,sta} = Q_{a,sta} + Q_{b,sta} = Q_{out,sta} \quad (1)$$

where $Q_{in,sta}$ and $Q_{out,sta}$ represent the total inlet air flow rate and the total outlet air flow rate of the system, respectively. $Q_{1,sta}$, $Q_{2,sta}$, $Q_{3,sta}$, and $Q_{4,sta}$ are the inlet air flow rate of the FR distributor, the fluidizing air flow rate of the J-valve, the aeration air flow rate of the J-valve, and the inlet air flow rate of the AR, respectively. $Q_{a,sta}$ and $Q_{b,sta}$ are the outlet air flow rates of the FR and the AR, respectively.

All the inlet/outlet gas flow rates mentioned above were measured by calibrated rotameters except $Q_{a,sta}$ which can be deduced from Equation (1).

$$Q_{a,sta} = Q_{1,sta} + Q_{2,sta} + Q_{3,sta} + Q_{4,sta} - Q_{b,sta} \quad (2)$$

The FR superficial gas velocity can be calculated as:

$$U_{f,sta} = \frac{Q_{f,sta}}{A_f} \tag{3}$$

where A_f is the sectional area of the FR. $Q_{f,sta}$ represents the total inlet air flow rate of the FR, which can be estimated as:

$$Q_{f,sta} = Q_{1,sta} + Q_{2,sta} + (1 - f_3)Q_{3,sta} \tag{4}$$

where f_3 represents the J-valve leakage ratio, and a detailed explanation of this parameter can be found in Section 2.4.3.

2.4.2. Solid Circulation Flux

The solid circulation flux can be estimated as:

$$G_s = \frac{\rho_b u_s A_d}{A_f} = \frac{\rho_b A_d}{A_f}(\Delta H/t) \tag{5}$$

where ρ_b, u_s, and A_d represent the bulk density of the OC, the downward flow velocity of the OC particles in the upper dipleg, and the sectional area of the upper downcomer, respectively. ΔH is a scale height in the upper dipleg for the measurement of solid circulation flux, and t is the measured duration of the traced OC particles passing through the scale height.

2.4.3. Gas Leakage Ratios

The distribution of the FR exhaust gas can be measured through the use of tracer gas 1. f_1, named as FR leakage ratio, represents the gas leakage ratio of the FR into the AR [31].

$$f_1 = \frac{Q_{b,sta}x_{b,CO}}{Q_{a,sta}x_{a,CO} + Q_{b,sta}x_{b,CO}} \tag{6}$$

where $x_{a,CO}$, and $x_{b,CO}$ are the concentrations of tracer gas 1 measured at the outlets of the separator and the AR, respectively.

Similarly, the distribution of the exhaust gas from the AR inlet can be investigated by using tracer gas 2. f_2, named as the AR leakage ratio, represents the gas leakage ratio of the AR into the FR [31].

$$f_2 = \frac{Q_{a,sta}x'_{a,CO}}{Q_{a,sta}x'_{a,CO} + Q_{b,sta}x'_{b,CO}} \tag{7}$$

where $x'_{a,CO}$ and $x'_{b,CO}$ are the concentrations of tracer gas 2 measured at the outlets of the separator and the AR, respectively.

Moreover, the distribution of the J-valve aeration air can be measured by the use of tracer gas 3. f_3, the so-called J-valve leakage ratio, represents the gas leakage ratio of the aeration air into the AR.

$$f_3 = \frac{Q_{b,sta}x''_{b,CO}}{Q_{a,sta}x''_{a,CO} + Q_{b,sta}x''_{b,CO}} \tag{8}$$

where $x''_{a,CO}$ and $x''_{b,CO}$ are the concentrations of tracer gas 3 measured at the outlets of the separator and the AR, respectively.

2.4.4. Gas Flow Rates

The upper pressure gradient ($\Delta P_1/H_1$) represents the pressure gradient between the AR and the separator.

$$\Delta P_1/H_1 = \left(\frac{P_b + P_c}{2} - P_i\right)/H_1 \quad (9)$$

where P_b and P_c are the pressures of the AR outlet and inlet, respectively. P_i represents the pressure at the top position of the upper dipleg of the AR, i.e., the pressure at the interface of the dense phase and dilute phase of the upper downcomer. As the pressure loss is very small in the dilute phase region of the upper downcomer, the value of P_i can be approximated by the pressure at the underside of the separator (i.e., P_{11}). H1 is the solid-seal height of the upper dipleg of the AR.

The lower pressure gradient ($\Delta P_2/H_2$) represents the pressure gradient between the J-valve and AR.

$$\Delta P_2/H_2 = (P_d - P_{12})/H_2 \quad (10)$$

where P_d is the pressure at the bottom position of the lower dipleg of the AR, and P_{12} the pressure at the top position of the lower dipleg. H_2, named as the solid-seal height of the lower dipleg, is represented by the height difference between the pressure monitoring nodes P_{12} and P_d.

3. Results and Discussion

As shown in Table 2, experiments were carried out with wide ranges of operating conditions (e.g., solid mass flux, superficial gas velocity, and pressure gradients) in order to present the primary flow behaviors of the proposed iG-CLC system. Thereinto, the operating condition of G_s = 310 kg/m^2·s, $U_{f,sta}$ = 10.7 m/s, $Q_{4,sta}$ = 48 m^3/h is defined as the reference condition which realized a balanced operation but involved relatively obvious gas leakage features to facilitate the observation and analysis.

Table 2. Main operation conditions of the iG-CLC tests.

Description	Range of Values
Solid circulation flux G_s (kg/m^2·s)	170–480
FR superficial gas velocity $U_{f,sta}$ (m/s)	7–12
AR inlet air flow rate $Q_{4,sta}$ (m^3/h)	20–60
Upper pressure gradient $\Delta P_1/H_1$ (kPa/m)	−4–13
Lower pressure gradient $\Delta P_2/H_2$ (kPa/m)	2.0–7.0

3.1. Pressure Balance and Solid Circulation of the iG-CLC System

An appropriate pressure balance is vital to the balanced gas flow and solid circulation in an iG-CLC system; therefore, 19 pressure measuring nodes were mounted on the main assembly, the labels can be seen in Figure 2. Figure 3 shows the pressure profile of the system under the reference condition. It can be found that the sum of the pressure drop within a solid circulation loop was zero. This indicates the whole system was self-stabilizing and hence a small perturbation would not break the balance of solid circulation. The pressure drop along the height of the FR was conspicuous with the total pressure difference between P_1 at the bottom and P_{10} at the top reaching up to 12.8 kPa. In contrast, the pressure drop of the AR (i.e., $P_c - P_b$) was only about 1.5 kPa with a CFMB structure.

Due to the coupling of the AR in the middle of the downcomer, the dipleg of the downcomer was divided into two parts, the upper dipleg and the lower dipleg of the AR. Here, we adopted H_1, see Figure 2, as the solid-seal height of the upper dipleg and H_2, see Figure 2, as the solid-seal height of the lower dipleg. As shown in Figure 3, the pressures of the two diplegs both linearly increased from top to bottom, indicating that the solid flow structures in the two diplegs under the reference condition both belonged to the negative pressure differential flow. Moreover, the existence of the AR made the pressure distributions of the two diplegs relatively independent of each other. To be specific, the pressure distribution along the upper dipleg was mainly determined by the outlet pressures of

the AR and FR, and the solid-seal height of the upper dipleg (i.e., H_1), while the pressure distribution along the lower dipleg was determined by the pressures of the AR and the J-valve together with the solid-seal height of the lower dipleg (i.e., H_2).

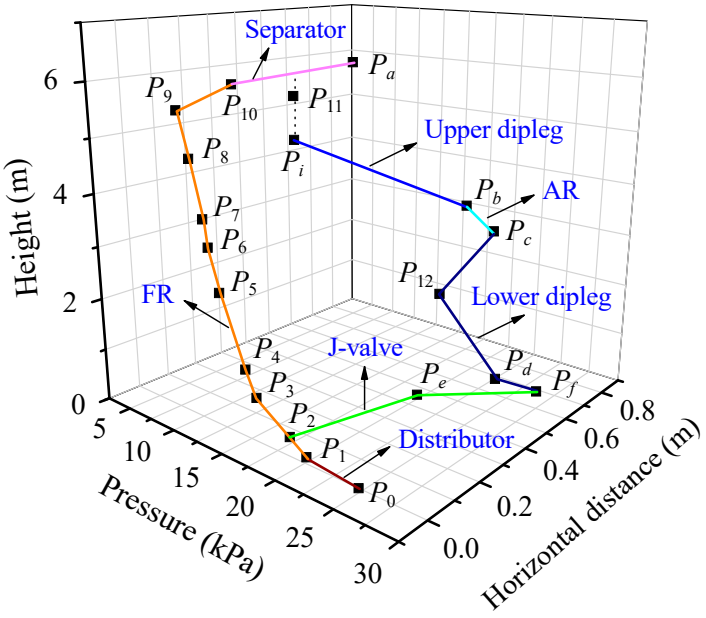

Figure 3. Pressure profile of the iG-CLC system under the reference condition.

The solid circulation rate is significant to the performance of an iG-CLC system, which determines the carrying capacity of oxygen and heat transferred by the OC from the AR to the FR. Figure 4 shows the distributions of the solid circulation flux G_s corresponding to the FR superficial gas velocity $U_{f,sta}$. It can be seen that a wide range of G_s from 170 to 480 kg/m^2·s had been achieved, indicating a good adaptability of this iG-CLC system on the OC circulation flux. This also demonstrates the positive role of the direct coupling method of the AR in the stabilization and controllability of the whole system. Thus, in the hot operation process, this iG-CLC system can achieve the feasible adjustment of oxygen and heat transfer according to actual situations. In particular, the capacity of high solid circulation flux ($G_s \geq 200$ kg/m^2·s) can greatly increase the OC inventory in the FR, and thus compensate for the possible low reactivity of the OC. Therefore, this iG-CLC system also provides the feasibility of the use of low-grade natural iron ores with lower reactivity than the OCs.

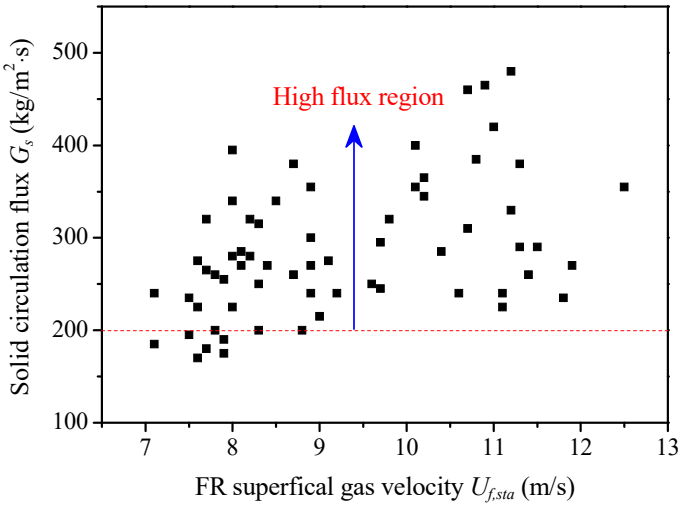

Figure 4. Distributions of the solid circulation flux corresponding to the FR superficial gas velocity.

3.2. Effect of the AR Coupling on the Solid Circulation

The direct coupling of the CFMB AR into the HFCFB system will inevitably affect the gas-solid flow behaviors of the system. In our previous work, we indeed notice that the OC circulation seemed to be affected during the adjustment process of the AR back pressure [31]. Therefore, it is significant to understand the fundamental effects of the AR coupling on the flux and further the stability of OC circulation.

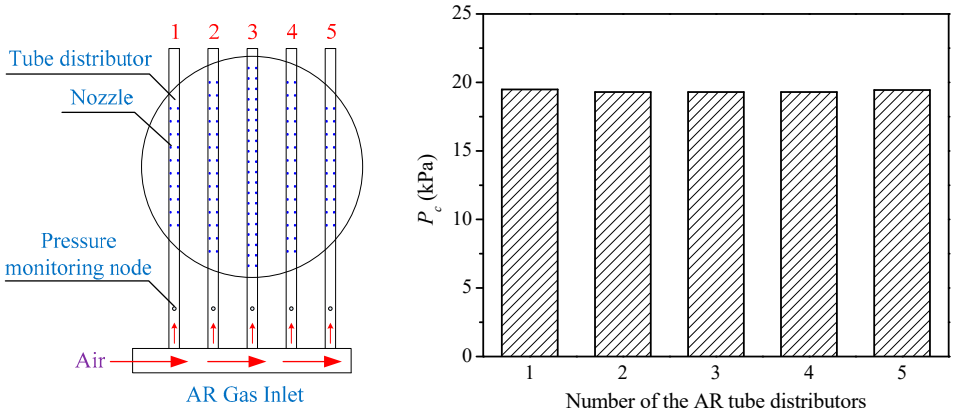

Figure 5. Pressure profiles of the parallel AR tube distributors under the reference condition: (**a**) schematic of the AR tube distributors, and (**b**) pressure profiles.

Figure 5 shows the pressure profiles of the parallel AR tube distributors under the reference condition. It can be seen that the inlet pressures of the five distributors were basically the same, demonstrating the realizability of even flow and distribution of gas-solid phases in the AR under certain conditions. In this context, a series of tests were carried out to investigate the fundamental effects of the AR coupling on the OC circulation flux and the system stability. We found that the OC circulation was actually determined by more factors that had interactions with each other (e.g., the pressures of the two reactors and the J-valve, the solid-seal heights above and under the AR), not just the AR back pressure. Here, we proposed a combined influence factor, the so-called upper pressure gradient $\Delta P_1/H_1$, which integrated the pressures of the two reactors and the solid-seal height of the upper dipleg, and hence should be able to more reasonably reflect the characteristics of OC circulation. Figure 6a shows the variations of the solid circulation flux with the upper pressure gradient $\Delta P_1/H_1$ while keeping all other parameters constant. It can be seen that the whole process could be divided into three sequential stages. In the first stage (-3.3 kPa/m $\leq \Delta P_1/H_1 \leq$ 8.90 kPa/m), the solid circulation flux had a linear increase from 215 to 260 kg/m^2·s with the increase of $\Delta P_1/H_1$, which was defined as the stage of circulation strengthening. In the second stage (8.9 kPa/m $< \Delta P_1/H_1 <$ 10.7 kPa/m), the so-called transition stage, the solid circulation flux began to decrease. In the third stage ($\Delta P_1/H_1 \geq$ 10.7 kPa/m), the solid circulation flux would drastically decline until the circulation collapsed completely, which was defined as the stage of circulation collapse.

The above results indicated that, with the increase in the upper pressure gradient $\Delta P_1/H_1$, the solid circulation flux would increase initially and later decrease until the circulation collapsed. First, in the stage of circulation strengthening, the material seal of the upper dipleg could overcome most of the gas leakage from the AR to the separator in spite of the increase of the upper pressure gradient. Better still, the increasing upper pressure gradient due to the increase of the AR back pressure also gave rise to the decrease of the lower pressure gradient $\Delta P_2/H_2$, and further, the decline of the aeration air leakage ratio from the J-valve to the AR (i.e., f_3), which indirectly enhanced the driving force of the J-valve aeration air for the OC circulation, and hence led to the increase of solid circulation flux. Then, starting from the transition stage, the material seal of the upper dipleg would be gradually destroyed by the increasing upper pressure gradient with the creation of large bubbles in the upper dipleg, as

shown in Figure 6b (the bubbles were circled in red). The retrograde motion of the bubbles in the upper dipleg greatly blocked the downward flow of the OC, which was the reason the solid circulation of the whole system was broken. Worse still, the appearance of bubbles also meant the massive leakage of N_2 from the AR into the separator, and hence the great reduction in the CO_2 concentration. Given the above, under the operational conditions shown in Figure 6a, the upper pressure gradient $\Delta P_1/H_1$ should be limited to 8.9 kPa/m (i.e., within the stage of circulation strengthening), where the OC circulation was balanced and adjustable.

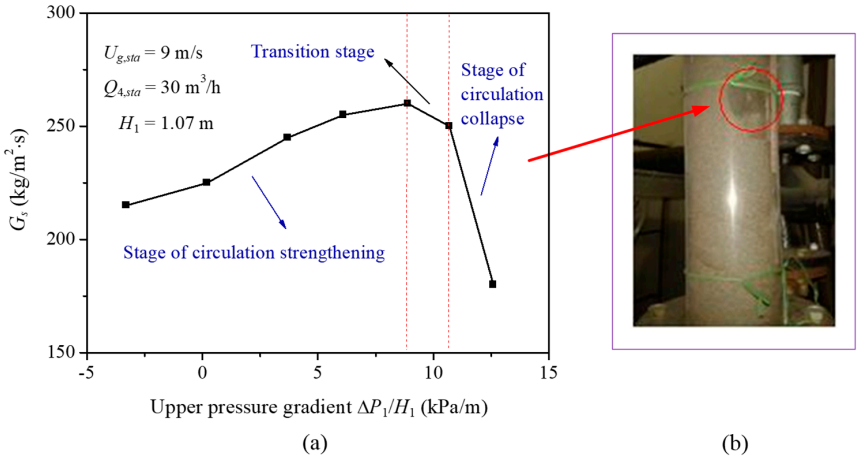

Figure 6. Variations of the solid circulation patterns with the upper pressure gradient: (**a**) variations of the solid circulation flux; and (**b**) snapshot of the state of circulation collapse.

3.3. Effect of the AR Coupling on the Gas Leakages

The gas leakages between reactors are one of the key factors affecting the performance of an iG-CLC system, such as the CO_2 capture efficiency, the CO_2 capture concentration, and even the solid circulation flux. As shown in Figure 7, there are three possible routes of gas leakages in our iG-CLC system: From FR to AR (i.e., FR leakage ratio f_1), from AR to FR (i.e., AR leakage ratio f_2), and from J-valve to AR (i.e., J-valve leakage ratio f_3). It can be found that the AR is the critical component associated with each leakage route. Hence, it is very meaningful to understand the influence mechanism of the AR coupling on the gas leakages in order to discover feasible solutions.

After a series of tests, the gas leakages were also found to be determined by the pressure gradients of the AR, which integrated the effects of the pressures of the two reactors and the J-valve, and the solid-seal heights of the upper and lower diplegs. Figure 8 shows the variations of the FR leakage ratio f_1 and the AR leakage ratio f_2 with the upper pressure gradient $\Delta P_1/H_1$ under a high solid flux condition (G_s = 200 kg/m^2·s). It can be seen that the FR leakage ratio f_1 could be effectively reduced with an increase in the upper pressure gradient $\Delta P_1/H_1$. When $\Delta P_1/H_1$ exceeded 0.7 kPa/m, the value of f_1 would decline to about zero, indicating the gas leakage from the FR to the AR had almost disappeared. However, we also observed a contrary trend of the AR leakage ratio f_2 with the upper pressure gradient $\Delta P_1/H_1$. First, f_2 was kept near zero when $\Delta P_1/H_1$ increased from -2.2 to 1.6 kPa/m, indicating the upper dipleg could seal the AR gas stream perfectly within this range of $\Delta P_1/H_1$. When $\Delta P_1/H_1$ exceeded 1.6 kPa/m, f_2 would rise rapidly, indicating the material seal in the upper dipleg began to gradually lose its effectiveness.

In the commercial application, if the FR leakage ratio f_1 is excessive, the CO_2 capture efficiency will be greatly reduced. Moreover, more unreacted char will be carried by the leaked gas of the FR into the AR for combustion, which will increase the risk of OC sintering, and further influence the operation stability of the whole system. On the other hand, if the AR leakage ratio f_2 becomes too large, a large amount of N_2 from the AR will bypass into the separator and mix with the FR exhaust gas, resulting in a substantial decrease in the CO_2 concentration. Worse still, the gas leakage may also impede the downward flow of the solid in the upper dipleg and break the system circulation stability,

as mentioned in Section 3.2. Therefore, both the FR leakage ratio f_1 and the AR leakage ratio f_2 must be limited to lower values. However, in view of the opposite effects of the upper pressure gradient $\Delta P_1/H_1$ on f_1 and f_2, a coordination control and optimized matching is inevitable. Under the involved operation conditions, the range of $\Delta P_1/H_1$ between -2.1 to 3.0 kPa/m should be an optimal region for adjustment, in which the values of f_1 and f_2 could be limited to 3%, together with a favorable solid circulation.

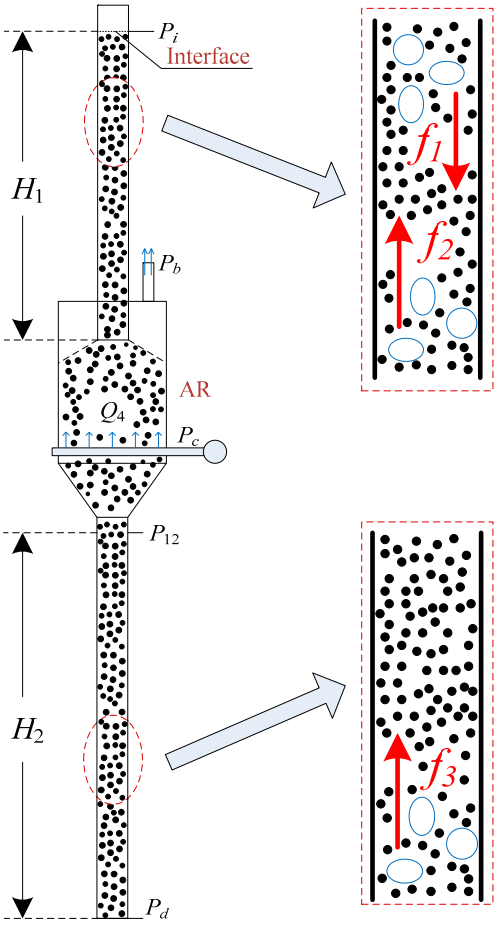

Figure 7. The possible routes of gas leakages in the proposed iG-CLC system.

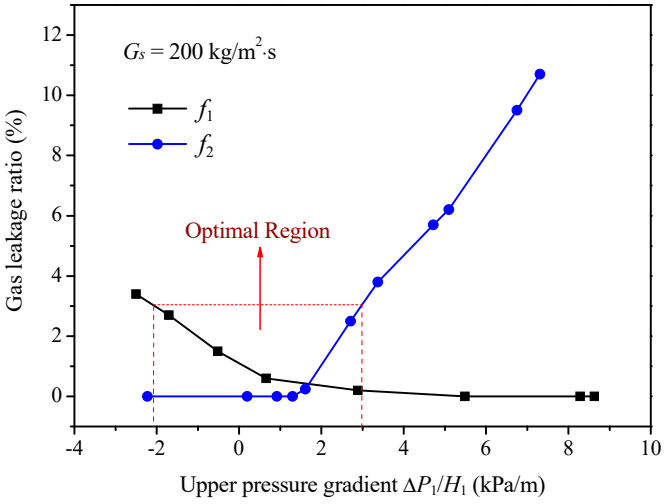

Figure 8. Variations of FR leakage ratio and AR leakage ratio with the upper pressure gradient.

On the other hand, the lower pressure gradient $\Delta P_2/H_2$ could be used to reflect the gas leakage ratio of the J-valve to the AR. Figure 9 presents the variations of the J-valve leakage ratio f_3 with the lower pressure gradient $\Delta P_2/H_2$. When the lower pressure gradient $\Delta P_2/H_2$ increased from 2.3 to 6.9 kPa/m, the J-valve leakage ratio f_3 had an obvious increase from 6.0% to 21.3% with a near-linear trend. This indicated a negative effect of the lower pressure gradient on the suppression of the gas leakage from the J-valve to the AR. In the iG-CLC application, a small amount of gas leakage from the J-valve to the AR will rarely affect the circulation stability of the system, and hence can be accepted. However, an excess gas leakage will cause the aeration gas stream of the J-valve to no longer contribute to the solid circulation, but impede the downward flow of the particles. Worse yet, the excess gas leakage will lower the air inflow to the AR, and hence reduce the thermal power of the proposed iG-CLC system. Therefore, under the involved operation conditions, the lower pressure gradient $\Delta P_2/H_2$ should be limited within 6.0 kPa/m, and thus the J-valve leakage ratio f_3 could also be controlled within a low value (20%) with a favorable solid circulation.

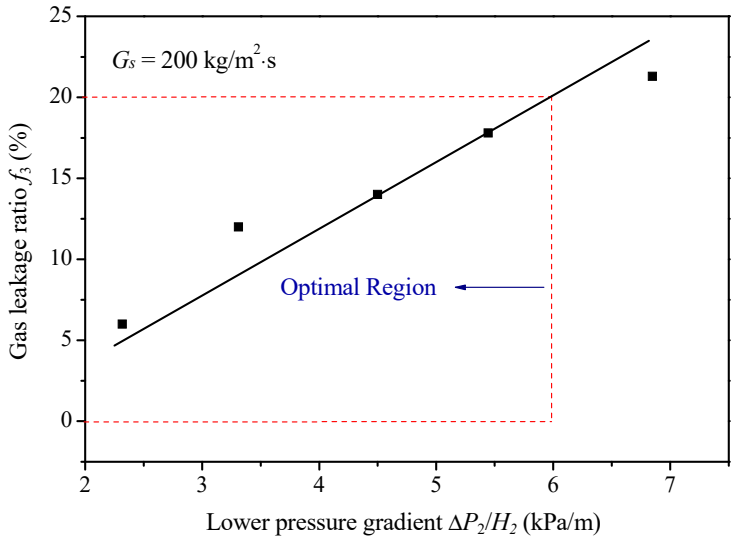

Figure 9. Variations of the J-valve leakage ratio with the lower pressure gradient.

3.4. Performance Optimization of the AR Coupling

Based on the above analysis, the coupling of the AR has important effects, by virtue of the upper pressure gradient $\Delta P_1/H_1$ and the lower pressure gradient $\Delta P_2/H_2$, on the characteristics of gas leakages and even the solid circulation stability. In the practical operation process, we can adjust the relevant parameters (i.e., the pressures of the two reactors and the J-valve, and the solid-seal heights in the downcomer) flexibly and optimally to guarantee the pressure gradients within the optimal ranges for an ideal performance of operation and reaction.

In order to better exhibit the effect of the AR coupling, we carried out a comparison of gas leakages between the reference condition and an optimal condition, as shown in Table 3. On the basis of the coupling criteria proposed in Section 3.3, the upper pressure gradient $\Delta P_1/H_1$ and lower pressure gradient $\Delta P_2/H_2$ in the optimal test were selected to be 3.5 kPa/m and 5.0 kPa/m, respectively. It could be found that for the reference condition, although achieving a balanced solid circulation in the whole system, an unsatisfactory gas leakage of the AR (i.e., f_2) was observed, indicating considerable mixing of N_2 from the AR into the FR exhaust gas stream, and hence an obvious reduction in the CO_2 concentration. However, the good news is that, with an optimization of the pressure gradients, the iG-CLC unit, under the optimal condition, inhibited the gas leakages, together with a favorable solid circulation. This demonstrates the significance of the study of the AR coupling mechanism in the high-flux iG-CLC system for the achievement of high CO_2 capture efficiency and

CO_2 capture concentration under a balanced system operation, which could provide vital information and experience for the design of future large-scale coal-fired CLC power plants.

Table 3. Comparison of gas leakages between the reference condition and optimal condition.

Description	Reference Condition	Optimal Condition
Solid circulation flux G_s (kg/m^2·s)	310	310
Upper pressure gradient $\Delta P_1/H_1$ (kPa/m)	8.0	3.5
Lower pressure gradient $\Delta P_2/H_2$ (kPa/m)	3.8	5.0
FR leakage ratio f_1 (%)	0	0
AR leakage ratio f_2 (%)	10.7	1.9
J-valve leakage ratio f_3 (%)	11.0	15.0

4. Conclusions

On the basis of the previous feasibility studies of a high-flux iG-CLC system, this work further investigated the AR coupling effects on the system operation stability and gas leakages with a cold-state visualization device, enabling the design parameters and operating conditions. The following conclusions can be drawn from the present study:

(1) The iG-CLC system exhibited favorable pressure distribution characteristics and good adaptability of solid circulation flux, demonstrating the positive role of the direct coupling method of the AR in the stabilization and controllability of the whole system.

(2) With the increase of the upper pressure gradient of the AR, the OC circulation flux would increase initially and later decrease until the circulation collapsed, demonstrating the crucial effect of the AR coupling on the OC circulation flux and further the circulation stability. In the real iG-CLC applications, the upper pressure gradient of the AR should be limited within the stage of circulation strengthening in order to guarantee a balanced and adjustable OC circulation.

(3) The gas leakage ratios of the FR and the AR were determined by the upper pressure gradient of the AR, while the gas leakage ratio of the J-valve was determined by the lower pressure gradient. In the iG-CLC applications, we can adjust the pressures of the two reactors and the solid-seal heights in the downcomer flexibly and optimally to ensure the two pressure gradients within the optimal ranges for an ideal balance of all the gas leakages.

(4) By giving consideration to the AR coupling effects under various operation conditions comprehensively, one operating condition with 3.5 kPa/m for the upper pressure gradient and 5.0 kPa/m for the lower pressure gradient was recommended. Under this condition, the gas leakages between the two reactors could be limited to 3%, and the gas leakage of the J-valve could also be below 20% to guarantee the solid circulation. This demonstrates the significance of the study of the AR coupling mechanism in the high-flux iG-CLC system for the achievement of high CO_2 capture efficiency and CO_2 capture concentration under a balanced system operation.

Author Contributions: X.W. conceived and designed the experiments; X.L. performed the experiments; X.W. and X.L. analyzed the data; B.J. supervised the research; X.W., X.L. and D.W. wrote the manuscript.

Funding: This research was funded by the National Natural Science Foundation of China (grant numbers 51741603, 51806035, 51676038), the Natural Science Fund project in Jiangsu Province (grant number BK20170669), the Fundamental Research Funds for the Central Universities (grant number 2242018K40117), and the Guangdong Provincial Key Laboratory of New and Renewable Energy Research and Development (grant number Y707s41001).

Conflicts of Interest: The authors declare no conflict of interest.

References

1. Fan, L.S.; Zeng, L.; Wang, W.; Luo, S. Chemical looping processes for CO_2 capture and carbonaceous fuel conversion—Prospect and opportunity. *Energy Environ. Sci.* **2012**, *5*, 7254–7280. [CrossRef]
2. Lyngfelt, A.; Leckner, B.; Mattisson, T. A fluidized-bed combustion process with inherent CO_2 separation; application of chemical-looping combustion. *Chem. Eng. Sci.* **2001**, *56*, 3101–3113. [CrossRef]

3. Abad, A.; Mattisson, T.; Lyngfelt, A.; Johansson, M. The use of iron oxide as oxygen carrier in a chemical-looping reactor. *Fuel* **2007**, *86*, 1021–1035. [CrossRef]
4. Mattisson, T.; García-Labiano, F.; Kronberger, B.; Lyngfelt, A.; Adánez, J.; Hofbauer, H. Chemical-Looping Combustion using syngas as fuel. *Int. J. Greenh. Gas Control* **2007**, *1*, 158–169. [CrossRef]
5. Ishida, M.; Jin, H.; Okamoto, T. A fundamental study of a new kind of medium material for chemical-looping combustion. *Energy Fuels* **1996**, *10*, 958–963. [CrossRef]
6. Jin, H.; Okamoto, T.; Ishida, M. Development of a novel chemical-looping combustion: Synthesis of a solid looping material of $NiO/NiAl_2O_4$. *Ind. Eng. Chem. Res.* **1999**, *38*, 126–132. [CrossRef]
7. Mattisson, T.; Järdnäs, A.; Lyngfelt, A. Reactivity of some metal oxides supported on alumina with alternating methane and oxygen application for chemical-looping combustion. *Energy Fuels* **2003**, *17*, 643–651. [CrossRef]
8. Cho, P.; Mattisson, T.; Lyngfelt, A. Comparison of iron-, nickel-, copper-and manganese-based oxygen carriers for chemical-looping combustion. *Fuel* **2004**, *83*, 1215–1225. [CrossRef]
9. Abad, A.; Mattisson, T.; Lyngfelt, A.; Rydén, M. Chemical-looping combustion in a 300 W continuously operating reactor system using a manganese-based oxygen carrier. *Fuel* **2006**, *85*, 1174–1185. [CrossRef]
10. De Diego, L.F.; García-Labiano, F.; Gayán, P.; Celaya, J.; Palacios, J.M.; Adánez, J. Operation of a 10 kWth chemical-looping combustor during 200 h with a $CuO\text{-}Al_2O_3$ oxygen carrier. *Fuel* **2007**, *86*, 1036–1045. [CrossRef]
11. Adánez, J.; Dueso, C.; de Diego, L.F.; García-Labiano, F.; Gayán, P.; Abad, A. Methane combustion in a 500 Wth chemical-looping combustion system using an impregnated Ni-based oxygen carrier. *Energy Fuels* **2008**, *23*, 130–142. [CrossRef]
12. Kolbitsch, P.; Bolhàr-Nordenkampf, J.; Pröll, T.; Hofbauer, H. Operating experience with chemical looping combustion in a 120 kW dual circulating fluidized bed (DCFB) unit. *Int. J. Greenh. Gas Control* **2010**, *4*, 180–185. [CrossRef]
13. Ma, J.; Zhao, H.; Tian, X.; Wei, Y.; Zhang, Y.; Zheng, C. Continuous Operation of Interconnected Fluidized Bed Reactor for Chemical Looping Combustion of CH_4 Using Hematite as Oxygen Carrier. *Energy Fuels* **2015**, *29*, 3257–3267. [CrossRef]
14. Diglio, G.; Bareschino, P.; Mancusi, E.; Pepe, F. Techno-Economic Evaluation of a small-scale power generation unit based on a Chemical Looping Combustion Process in Fixed Bed Reactor network. *Ind. Eng. Chem. Res.* **2018**, *57*, 11299–11311. [CrossRef]
15. Cao, Y.; Pan, W.P. Investigation of Chemical looping combustion by solid fuels: 1 Process analysis. *Energy Fuels* **2006**, *20*, 1836–1844. [CrossRef]
16. Berguerand, N.; Lyngfelt, A. Design and operation of a 10 kW_{th} chemical-looping combustor for solid fuels-testing with South African coal. *Fuel* **2008**, *87*, 2713–2726. [CrossRef]
17. Leion, H.; Mattisson, T.; Lyngfelt, A. Solid fuels in chemical-looping combustion. *Int. J. Greenh. Gas Control* **2008**, *2*, 180–193. [CrossRef]
18. Shen, L.H.; Wu, J.H.; Xiao, J. Experiments on chemical looping combustion of coal with a NiO based oxygen carrier. *Combust. Flame* **2009**, *156*, 721–728. [CrossRef]
19. Fan, L.S.; Li, F. Chemical looping technology and its fossil energy conversion applications. *Ind. Eng. Chem. Res.* **2010**, *49*, 10200–10211. [CrossRef]
20. Abad, A.; Gayán, P.; de Diego, L.F.; García-Labiano, F.; Adánez, J. Fuel reactor modelling in chemical-looping combustion of coal: 1. Model formulation. *Chem. Eng. Sci.* **2013**, *87*, 277–293. [CrossRef]
21. García-Labiano, F.; de Diego, L.F.; Gayán, P.; Abad, A.; Adánez, J. Fuel reactor modelling in chemical-looping combustion of coal: 2-simulation and optimization. *Chem. Eng. Sci.* **2013**, *87*, 173–182. [CrossRef]
22. Thon, A.; Kramp, M.; Hartge, E.-U.; Heinrich, S.; Werther, J. Operational experience with a system of coupled fluidized beds for chemical looping combustion of solid fuels using ilmenite as oxygen carrier. *Appl. Energy* **2014**, *118*, 309–317. [CrossRef]
23. Bayham, S.; McGiveron, O.; Tong, A.; Chung, E.; Kathe, M.; Wang, D.; Zeng, L.; Fan, L.S. Parametric and dynamic studies of an iron-based 25-kW_{th} coal direct chemical looping unit using sub-bituminous coal. *Appl. Energy* **2015**, *145*, 354–363. [CrossRef]
24. Adánez, J.; Abad, A.; Perez-Vega, R.; Luis, F.; García-Labiano, F.; Gayán, P. Design and Operation of a Coal-fired 50 kW_{th} Chemical Looping Combustor. *Energy Procedia* **2014**, *63*, 63–72. [CrossRef]
25. Markström, P.; Linderholm, C.; Lyngfelt, A. Operation of a 100 kW chemical-looping combustor with Mexican petroleum coke and Cerrejón coal. *Appl. Energy* **2014**, *113*, 1830–1835. [CrossRef]

26. Ma, J.; Zhao, H.; Tian, X.; Wei, Y.; Rajendran, S.; Zhang, Y.; Bhattacharya, S.; Zheng, C. Chemical looping combustion of coal in a 5 kW_{th} interconnected fluidized bed reactor using hematite as oxygen carrier. *Appl. Energy* **2015**, *157*, 304–313. [CrossRef]
27. Ströhle, J.; Orth, M.; Epple, B. Design and operation of a 1 MW_{th} chemical looping plant. *Appl. Energy* **2014**, *113*, 1490–1495. [CrossRef]
28. Xiao, R.; Chen, L.; Saha, C.; Zhang, S.; Bhattacharya, S. Pressurized chemical-looping combustion of coal using an iron ore as oxygen carrier in a pilot-scale unit. *Int. J. Greenh. Gas Control* **2012**, *10*, 363–373. [CrossRef]
29. Wang, X.; Jin, B.; Zhang, Y.; Zhang, Y.; Liu, X. Three Dimensional Modeling of a Coal-Fired Chemical Looping Combustion Process in the Circulating Fluidized Bed Fuel Reactor. *Energy Fuels* **2013**, *27*, 2173–2184. [CrossRef]
30. Wang, X.; Jin, B.; Liu, X.; Zhang, Y.; Liu, H. Experimental investigation on flow behaviors in a novel in situ gasification chemical looping combustion apparatus. *Ind. Eng. Chem. Res.* **2013**, *52*, 14208–14218. [CrossRef]
31. Wang, X.; Jin, B.; Liu, H.; Wang, W.; Liu, X.; Zhang, Y. Optimization of in Situ Gasification Chemical Looping Combustion through Experimental Investigations with a Cold Experimental System. *Ind. Eng. Chem. Res.* **2015**, *54*, 5749–5758. [CrossRef]
32. Wang, X.; Jin, B.; Zhu, X.; Liu, H. Experimental Evaluation of a Novel 20 kW_{th} in Situ Gasification Chemical Looping Combustion Unit with an Iron Ore as the Oxygen Carrier. *Ind. Eng. Chem. Res.* **2016**, *55*, 11775–11784. [CrossRef]